Electric field induced phototransport in dye-doped semiconducting polymer

Sougata Mandal* and Reghu Menon
Department of Physics, Indian Institute of Science Bangalore 560012, India

(Received 19 February 2024; accepted 27 June 2024; published 9 July 2024)

Electric field induced phototransport of regioregular poly(3-hexylthiophene) [P3HT] and squaraine (SQ) dye-sensitized samples are studied in this paper. The relative variation of photoresponse spectra shows that the trap energetics and charge transport are modified in the presence of 1 wt% SQ dye. In the doped sample, the $S(V)/S(60V)$ ratio at 2.1 eV increases by a factor of 21 at 1800 V/cm, with a substantial increase in the photoresponse. The redistribution of the trap energy levels and enhancement in transport is associated with the variations in transit and relaxation times of carriers in the presence of the dye. The phase part of the signal consisting of photocapacitance is reduced and becomes less dependent on the optical energy in the doped sample. This is consistent with the absence of space charge contribution in dye-doped samples. The deconvoluted photoresponse signal by using Gaussian functions indicates that the trapping-detrapping processes are altered by the dye since only three Gaussian peaks are observed in the dye-doped sample. The deconvoluted photoresponse in the dye-doped sample indicates that the modified trapping-detrapping processes have enhanced the transport, which results in three Gaussian peaks.

DOI: 10.1103/PhysRevMaterials.8.075602

I. INTRODUCTION

In recent years, there has been considerable interest in semiconducting polymers from both basic science and industrial aspects because of their applications in electronic and photonic devices [1–5]. Facile and low-cost processing of semiconducting polymers facilitated a wide range of products [6–9]. However, the presence of intrinsic disorder and its role in charge transport is yet to be fully understood, as it limits the carrier mobility in these systems. Since it is known that traps play a major role in charge transport, the electric field dependent transport of photogenerated carriers provides insight into the fundamental conduction mechanism of carriers in these materials.

Phototransport is a complex phenomenon that includes optical absorption, photocarrier generations, and the electrical transport of generated carriers, in which recombination, trapping, and detrapping of carriers limit the performance in many devices [10]. The photogenerated carriers either recombine or contribute to photovoltaic signals depending upon the carriers' lifetime and the distribution of spatial and energetic trap sites [11]. The electric field dependent phototransport can investigate the role of energetic disorder that limits the overall transport mechanism [12]. Since the trapping-detrapping processes in these disordered quasi-one-dimensional polymeric chains are quite complex and sensitive to nanoscale morphology, the peaks and tails associated with the spectra can give insight into trap dynamics related to the energetic disorder and transport processes.

The onset of the increase in conductivity occurs near the absorption edge, and it subsequently decreases at a lower wavelength. This is observed to be field dependent even at low fields. The photoresponse can systematically follow the variations in both field and spectral wavelength. While the direct band-to-band transition is a fundamental characteristic of the materials, the trap density distribution profile can significantly alter the energetics involved in transport in disordered semiconductors. Aside from the primary photoexcitation features in the semiconductors, the transport of carriers in the trapping-detrapping processes controls the photoresponse, and its field dependence can probe the transport mechanism.

In this paper, the effect of the electric field dependence of photoresponse of both pristine and dye-doped regioregular poly(3-hexylthiophene) [P3HT] is carried out in the spectral range 300-850 nm. The measurements are carried out in the linear four probe configurations. The photovoltage is measured in the inner two probes by a lock-in amplifier, as the electric field is applied to the outer two probes, in this four-probe method. Even at low field variations, a systematic change in the photoresponse can be observed; and this is significantly altered by adding a small volume fraction of a photosensitizer. The variation in the signal with field can probe the role of space charge and associated trapping-detrapping processes in phototransport, as the presence of squaraine (SQ) molecules alters the trap-related processes involved in the transport. The field dependence of photocapacitance is decreased in the presence of the dye. The deconvoluted spectral features in pristine P3HT by Gaussian functions give insight into the shallow, intermediate, and deep trap states profile. The qualitative features in the trap dynamics can be evaluated by using this analysis.

The goal of this paper is to develop a four-probe method to investigate phototransport in semiconducting polymers, and this could improve the understanding of photophysics in semiconducting polymers. Since it is known that a wide

*Contact author: sougatam@iisc.ac.in

range of distribution of trap states in any disordered semiconductors can significantly affect the phototransport, this method can accurately measure the real and imaginary parts of the signal, representing photoconductivity and photocapacitance, respectively. In this paper, the feasibility of the four-probe phototransport is shown in both pristine and dye-doped samples. Furthermore, the quantification of the trapping-detrapping times, transit time, and activation energy is expected to give more insight, and this is aimed at future work.

II. EXPERIMENTAL METHODS

A. Materials and experimental design

Regioregular P3HT (Merk) solution of concentration 3.5 mg/ml is prepared in chlorobenzene. In the P3HT-SQ sample, 1 wt% SQ dye is added to the P3HT solution. The solution is drop-casted on a 1 cm × 1 cm glass substrate for samples of thickness 1–10 μm. The transmission spectra of both pristine and dye-doped samples are shown in Fig. S1 within the Supplemental Material (SM) [13]. Four colinear aluminum (Al) contacts of thickness 100 nm are deposited by thermal evaporation using a shadow mask, with contact separations of 1 mm {as shown in Fig. S2(a) within the SM [13]}. Outer probes are used to apply an electric field, whereas light source from a monochromator (300–850 nm) incidence on the gap between two inner probes. Electric field-dependent photoresponse is measured using standard photomodulation techniques, as shown in the supplementary information [13], Fig. S3. Acton-2300i monochromator with a 150-W tungsten-halogen source is used to illuminate the sample in the energy range 1.5–4.0 eV. The monochromatic ray from the exit slit of Acton-2300i is chopped at 19 Hz using an optical chopper (model SR 540) before the incidence on the sample surface. The optically chopped monochromatic light ray is focused using a converging lens with a beam spot size of 1 mm on the gap between the two inner probes in the sample. The DC voltage across the outer electrodes is applied using a Keithley source-meter unit (SMU 2400), and the photovoltaic signal is detected by using a lock-in amplifier (SR830). The photovoltaic signal is collected by sweeping the monochromatic wavelength at a fixed electric field. The whole experimental setup is controlled, and data is acquired by the LabVIEW program connected to a PC (see Fig. S3 within the SM [13]).

B. Equivalent model

The equivalent circuit of electric field dependent photoconductivity measurements is shown in Fig. S2(b) within the SM [13]. The photovoltage response across the inner electrode S(V) can be calculated as

$$S(V) = V_{\text{ill}} - V_d = V\left(\frac{R_{\text{ill}}}{2R_d + R_{\text{ill}}} - \frac{1}{3}\right) = \frac{2V{R_d}^2 R_{\text{ill}}}{(2R_d + R_{\text{ill}})^2}\left(\frac{R_{\text{ill}} - R_d}{R_{\text{ill}}R_d}\right) \quad (1)$$

where V_{ill} is the illuminated sample voltage and V_d is the voltage when the sample is in the dark. V is the applied DC voltage. When the variation in the resistance of the sample in the dark (R_d) and in illumination (R_{ill}) becomes small, i.e., $R_d \approx R_{\text{ill}}$; Eq. (1) can be approximated to

$$S(V) = \frac{2}{9}VR_d\left(\frac{R_{\text{ill}} - R_d}{R_{\text{ill}}R_d}\right). \quad (2)$$

The difference in the conductance caused by the illumination is given by

$$\left(\frac{R_{\text{ill}} - R_d}{R_{\text{ill}}R_d}\right) = R_d^{-1} - R_{\text{ill}}^{-1} = \frac{9}{2}\frac{S(V)}{VR_d}. \quad (3)$$

Equation (3) is used to calculate the change in conductance value at different electric fields. The detailed discussion about the four-probe experiments is given within the SM [13].

III. RESULTS AND DISCUSSIONS

A. Photoresponse and comparision

Figure 1(a) shows the increase in photoresponse at the absorption edge of P3HT and its variation with the electric field. The systematic increase in photovoltage can be observed as the electric field is increased from 600 to 1800 V/cm. The sharp onset of the photovoltaic signal at 1.8 eV is observed in Fig. 1(a), indicating the π–π^* transition. The increase in peak shows that more carriers contribute to the photovoltage at the higher electric field. The increase in sharpness of the photovoltage at higher fields indicates that the distribution of the time scales involved in the trapping-detrapping processes is less broadened. The calculated change in $(R_d^{-1} - R_{\text{ill}}^{-1})$ in P3HT by using Eq. (3), as a function of optical energy at different electric fields, is shown in the inset of Fig. 1(a). The maxima in $(R_d^{-1} - R_{\text{ill}}^{-1})$ increases with electric field (600 to 1000 V/cm), and then it decreases slightly at higher fields (1000 to 1800 V/cm), as observed in the inset of Fig. 1(a). This decrease at higher fields is attributed to the formation of the space charge within the bulk of the sample. Figure 1(b) shows the variation in the phase part of the signal, arising from the capacitive contribution of the photogenerated carriers and this is associated with the trapping-detrapping processes when the optical energy and electric filed are varied. As the electric field increases, more carriers are detrapped and contribute to the photovoltage. The inset of Fig. 1(b) shows the corresponding increase in photocapacitance with the field, near the absorption edge. The photogeneration of carriers and associated trapping processes is observed as a peak in the photocapacitance at the band edge, as shown in the inset of Fig. 1(b). Also, the increase in photovoltage is mainly because of the enhanced carrier mobility at higher fields, although the variation of field is only by a factor of three. The decay in photovoltage in Fig. 1(a) indicates that the trapping of carriers is becoming more dominant; at the same time, the phase data in Fig. 1(b) change sign to negative values. However, the small values of the phase angle in Fig. 1(b) suggest that the photocapacitance contribution is less dominant when compared to the photovoltaic signal.

It is known that the SQ dye shows absorption maxima at 1.92 eV, which is rather close to the absorption peak in P3HT (see the transmission spectra in Fig. S1 within the SM [13]). Hence, SQ dye is an ideal photosensitizer for P3HT, and it mixes well with P3HT at low-volume fraction [14].

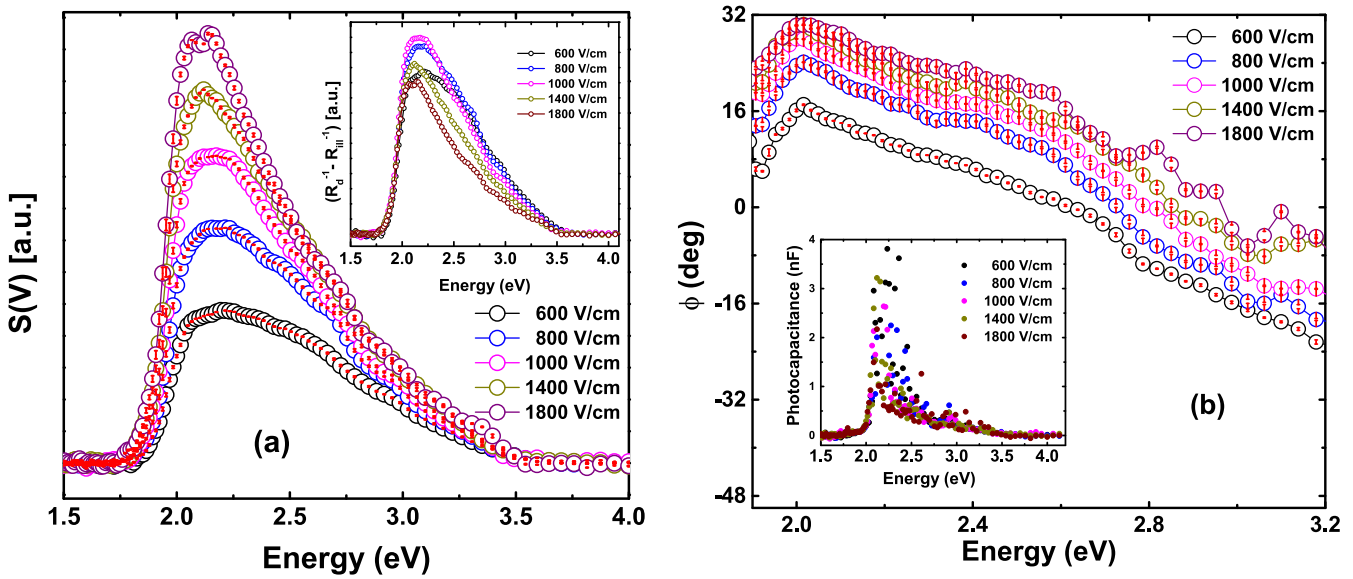

FIG. 1. (a) Electric field induced photoresponse of P3HT. Inset shows the variations in the optical energy $(R_d^{-1} - R_{\text{ill}}^{-1})$ at different electric fields. (b) The phase difference during phototransport measurements. Inset shows the photocapacitance contributions during phototransport measurements.

This provides a route to investigate the variation in phototransport in P3HT in the presence of photosensitizer. The electric field induced photoresponse for SQ dye-sensitized P3HT is shown in Fig. 2(a). This effect can be observed even at the low-volume fraction of 1 wt% of SQ. In P3HT-SQ, the measured photoresponse increases with the electric field and the onset of this increase occurs at 1.9 eV, associated with the absorption caused by dye molecules altering the π–π^* transition [15]. The effect of the electric field on the tail part of the photoresponse is prominent, and it broadens in the presence of dye. For instance, at 1800 V/cm, the tail part of the signal is quite well separated from the rest. This indicates that the effect of the electric field in phototransport is becoming more dominant, as the dye molecules facilitate more efficient energy transfer that affects trapping-detrapping processes. The calculated change in $(R_d^{-1} - R_{\text{ill}}^{-1})$ in P3HT-SQ by using Eq. (3) is shown in the inset of Fig. 2(a). In this case, the maxima in $(R_d^{-1} - R_{\text{ill}}^{-1})$ consistently increases with the field, and it becomes more prominent at 1800 V/cm. This variation in the inset of Fig. 2(a), compared to the spectra in the inset of Fig. 1(a), is because of the diminished role of space charge in trapping-detrapping processes in the doped

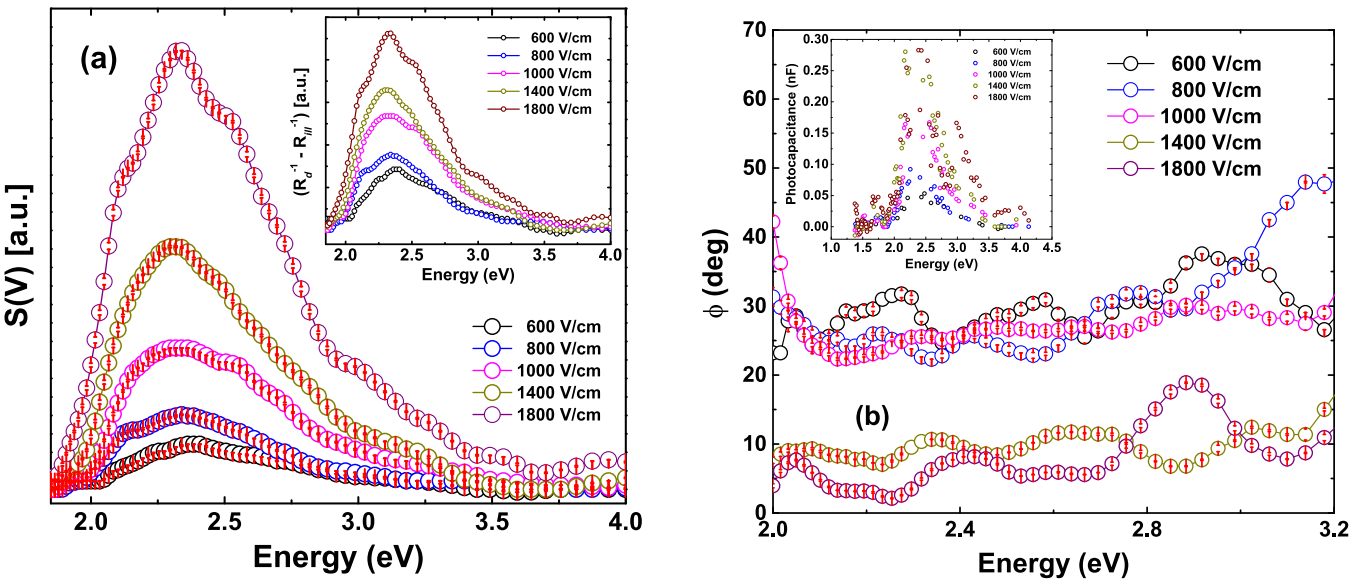

FIG. 2. (a) Electric field induced photoresponse of P3HT-SQ. Inset shows the variations with in optical energy $(R_d^{-1} - R_{\text{ill}}^{-1})$ at different electric fields. (b) The phase difference during phototransport measurements. Inset shows the photocapacitance contributions during phototransport measurements.

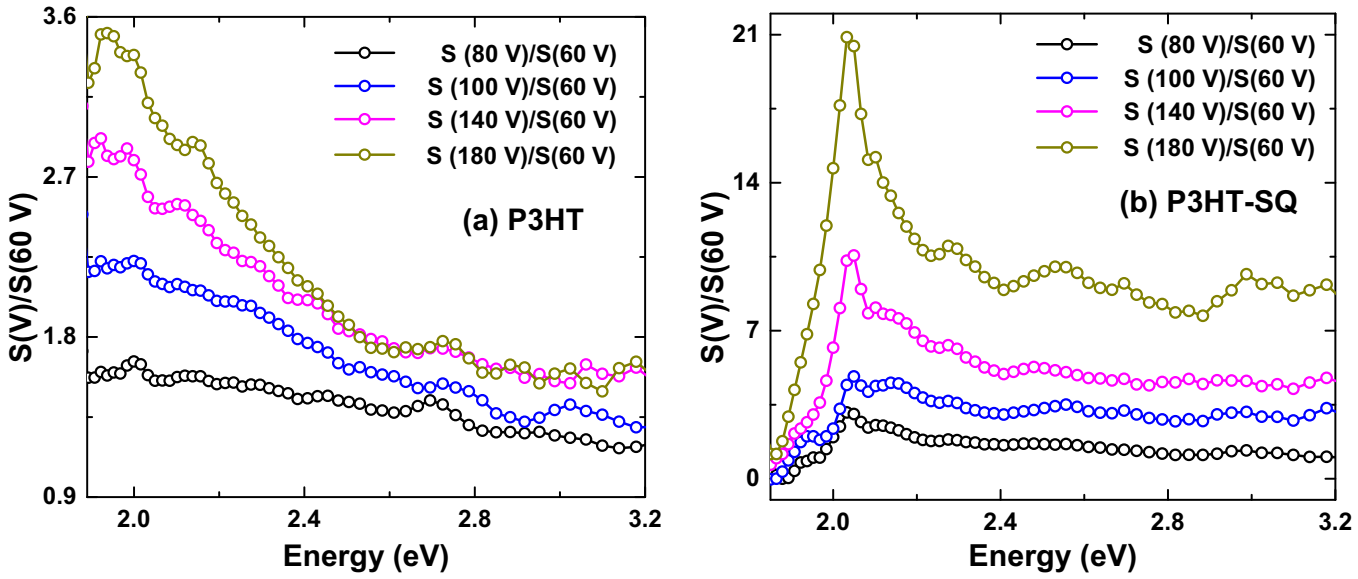

FIG. 3. The change in S(V)/S(60 V) ratio in the electric field induced photoresponse of (a) P3HT and (b) P3HT-SQ samples.

sample. The variation of the phase part of photoresponse is shown in Fig. 2(b), which is quite distinct from Fig. 1(b); and it hardly shows any significant variation with the energy, even at a higher electric field. The inset of Fig. 2(b) shows the photocapacitane contributions to the photoresponse. The maximum value is only 0.3 nF, much less than in P3HT, i.e., 4 nF. The nearly flat response of the phase signal in Fig. 2(b) indicates that trapping and detrapping processes are attaining a sort of quasi-equilibrium. This shows that photosensitization is a good method to investigate energy transfer and charge transport mechanisms in semiconducting polymers.

The effect of the electric field on the photoresponse becomes more relevant after normalizing the data with respect to the low field data at 600 V/cm, as the relative variation in the phototransport can be observed in this method. The relative changes in photovoltage [(S(V)/S(60 V)] for the entire spectral range at different electric fields are shown and compared in Figs. 3(a) and 3(b), for both P3HT and P3HT-SQ samples. With the increase of the electric field, the S(V)/S(60 V) ratio of the photoresponse increases in both films, as observed in Figs. 3(a) and 3(b). In the P3HT sample, as shown in Fig. 3(a), a slight increase in this ratio can be observed near 2.0 eV, and it increases at 1800 V/cm. However, in the P3HT-SQ sample, the peak at 2.04 eV is clearly seen, and this becomes more prominent at higher fields. The tail part of the data beyond 2.2 eV, in Fig. 3(b), becomes more flat, compared to Fig. 3(a). The maximum relative changes in photoresponse for P3HT at 180 V is only by a factor of 3.5, whereas for P3HT-SQ, this value is 21. This substantial increase by a factor of six in the latter is caused by the redistribution of the trap energetics, and this enhances the charge transport in the entire bulk of the sample. This clearly shows that the dynamics associated with trapping-detrapping processes have undergone a major change in the presence of the dye, plausibly associated with the time constants involved in the transport mechanism, and this aspect needs more detailed investigations in the future.

B. Electric field dependence

In the spectra in the inset of Fig. 1(a), $(R_d^{-1} - R_{\text{ill}}^{-1})$ changes as a function of both optical energy and the electric field, as in Eq. (2); and the selected values in the range 2.06–2.75 eV are used to fit the data as a function of the electric field. The plot of $S(V)$ vs electric field for P3HT is shown in Fig. 4(a). The data shows two different slopes as a function of electric fields. This change in slope in the power law fit $[S(V) \propto F^n]$ at around 1000 V/cm is attributed to the role of space charge in charge transport at higher fields. The value of n in the fit changes from 0.83 to 1.45 at the lower field, while $n = 0.25$–0.60 at higher fields in the log-log plot. This change in slope at the higher field is associated with the variation in carrier transit time compared to the relaxation time. At the lower electric field, the carrier transit time is more compared to the dielectric relaxation time, whereas, at the higher electric field, the carrier transit time reduces with respect to the relaxation time. These characteristics in charge transport are already known from previous impedance study [16]. The plot of $S(V)$ vs electric field for P3HT-SQ is shown in Fig. 4(b) and the value of $n =$ 2.0–2.5, in the log-log plot, with no change in slope as a function of the field. This shows that the carrier transit time and relaxation time are becoming constant and become comparable throughout the bulk in the dye-doped sample. As a result, the trapping-detrapping processes attain a quasi-equilibrium state, and this corroborates with the nearly flat response in the phase part of the signal, as a function of the field [see Fig. 2(b)]. This becomes more evident from the $S(V)/S(60V)$ plot as a function of the electric field, at different optical energy values, as shown in Fig. 4(c). The photoresponse signal increases with the electric field in both P3HT and P3HT-SQ samples, as observed in Fig. 4(c). In the dye-doped sample, the rate of increase is rapid, compared to the pristine P3HT sample. At 1800 V/cm, the ratio of the $S(V)/S(60V)$ signal is enhanced by a factor of 6, at 2.06 eV optical energy. This enhanced phototransport in the dye-doped sample is plausibly associated with the attainment of a quasi-equilibrium state,

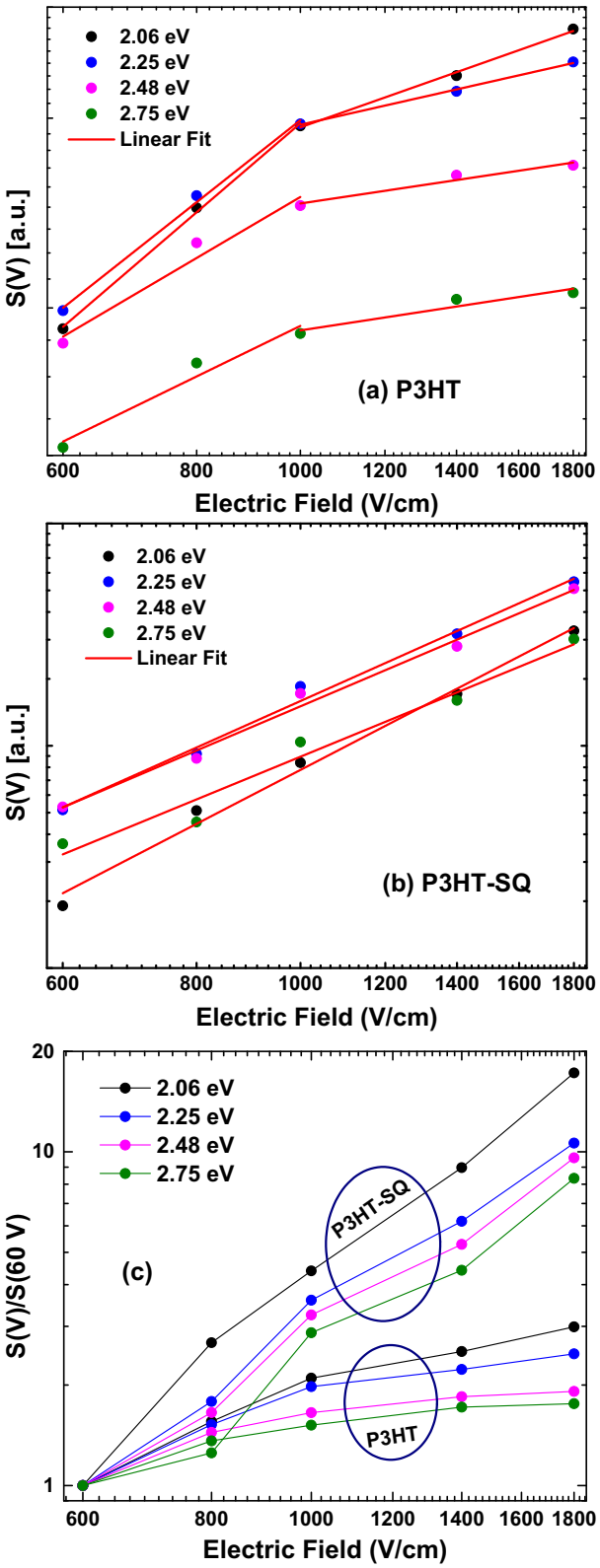

FIG. 4. Photoresponse at different illuminated optical energy as a function of electric field for (a) P3HT and (b) P3HT-SQ sample. This is fitted using power law, $S(V) \propto F^n$. (c) The change in $S(V)/S(60V)$ ratio with the electric field for different illuminated optical energy values.

as the carrier transit time and dielectric relaxation time are altered, and this improves the phototransport.

C. Trapping-detrapping dynamics

The deconvoluted $S(V)$ spectra of P3HT at 1800 V/cm is shown in Fig. 5(a). The best fit is obtained by using four Gaussian functions, as shown in Fig. 5(a); the inset shows the fitted Gaussian peak energy position values. In these materials, because of complex nanomorphology, it is known that the traps consist of shallow, intermediate, and deep states with overlapping Gaussian profiles. Hence, use of the Gaussian equations to fit the data is quite appropriate [17–20]. The energetics involved in this wide range of trap distributions can be identified from the peak energy positions in the fit, as shown in the inset table of Fig. 5(a). The peak energy positions can be approximately identified with deep, intermediate, and shallow trap distributions. Since P3HT consists of both crystalline and amorphous phases with a wide range of interchain interactions, the categorizations of these broad distributions of the trap states by using the Gaussian profile are quite appropriate [21]. The peak value and shape of the profiles give an approximate estimate of these distributions and their influence on the phototransport processes. The deconvoluted $S(V)$ spectra of P3HT-SQ at 1800 V/cm is shown in Fig. 5(b). In this case, only three Gaussian functions are required for the cumulative fit in the $S(V)$ spectra. The inset of Fig. 5(b) shows the peak energy position of Gaussian fittings. This shows that the energetics involved in phototransport are modified in the presence of the dye. The variation from four to three Gaussian profiles in the dye-doped sample shows that a redistribution of the energetics involved among the trap states has occurred. Peak 1 at 2.18 eV in the pristine sample is mixed up with peak 2 in the dye-doped sample, with modifications in the other profiles, and its effects are observed in the phototransport.

The peak positions in the deconvoluted Gaussian functions at 2.03, 2.18, 2.44, and 2.84 eV [see inset of Fig. 5(a)] represent the variation in the trap-related energetics in the phototransport. These energy values give provide insights into the roles of various activation processes, although they are not directly measured. This also corroborates with the full width at half maxima (FWHM) of the Gaussian functions. The peak position and FWHM of the spectra give a qualitative description of the various contributions to the photoresponse. For instance, the FWHM is less broadened in the case of shallow traps, whereas it broadens more in the case of intermediate and deep trap states. The FWHM of the Gaussian function is more broadened in the case of deep traps, as it requires more activation energy, compared to the deconvoluted signals of 1 and 4. This shows that the relative variation in the activation energy is more in 1 while compared to 4 [see Fig. 5(a)]. This analysis is also consistent in the P3HT-SQ sample, as in Fig. 5(b). These deconvoluted Gaussian spectra represent the distributions of the random trap energy sites, which is quite ubiquitous in semiconducting polymers. The first Gaussian function is attributed to the fundamental $\pi - \pi^*$ transitions, whereas the second, third, and fourth Gaussian functions are mainly because of the shallow, intermediate, and deep trap

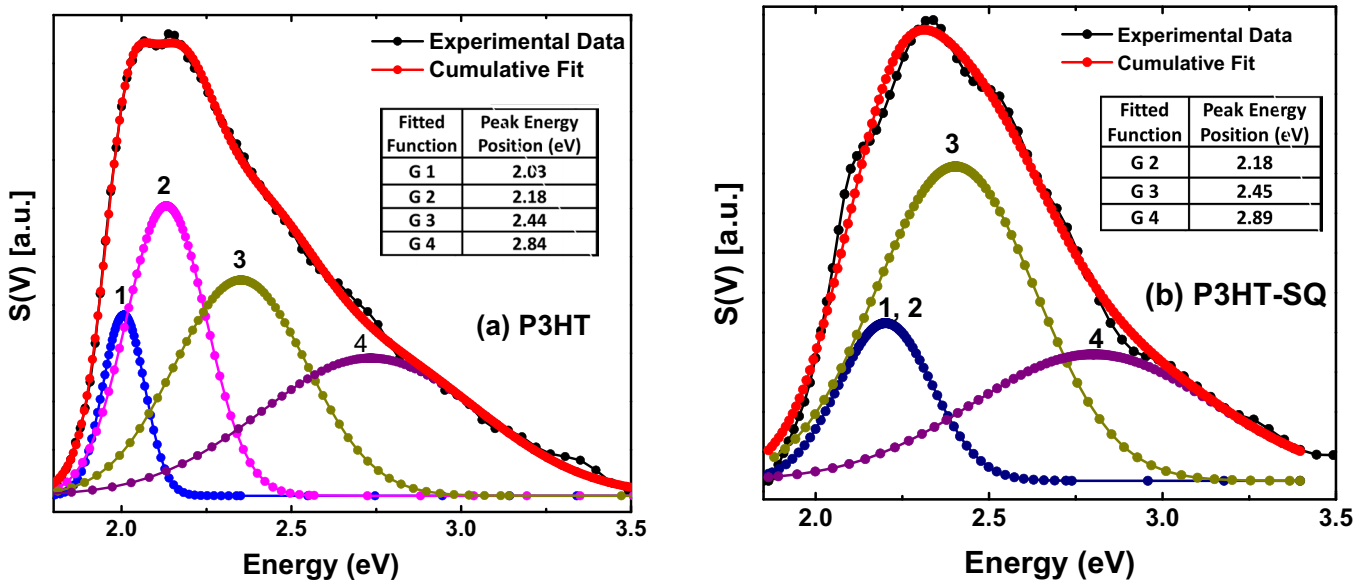

FIG. 5. Photoresponse spectra at 1800 V/cm as a function of optical energy is deconvoluted by using Gaussian functions for (a) P3HT and (b) P3HT-SQ samples. Insets show the peak energy values for fitted Gaussian functions.

states distributions, which arise from the nanoscale morphology in semiconducting polymers. With the addition of dye, the improved energy transfer processes is the main reason for the merging of peaks 1 and 2, as the energetics involved in $\pi - \pi^*$ transitions and the shallow trap distribution gets convoluted. This analysis corroborates with the $S(V)/S(60V)$ plots, as shown in Figs. 3(a), 3(b), and 4(c). It is observed that as optical energy increases the contributions from the intermediate and deep trap states reduce, and this results in the tails of the $S(V)/S(60V)$ spectra, as shown in Fig. 3(a).

IV. CONCLUSIONS

The effect of the squaraine dye in the phototransport of a semiconducting polymer (P3HT) is investigated by applying an electric field with a significantly improved signal-to-noise ratio by using a four-probe method. The modification of field-dependent spectra of phototransport in the presence of dye shows that the energetics associated with trap states alter the bulk transport. The S(V)/S(60 V) ratio at 1800 V/cm in the P3HT-SQ sample increases by a factor of 21 at 2.1 eV, which is nearly six times larger than in the P3HT sample. The onset of space charge is observed in the P3HT sample at around 1000 V/cm, and this feature is absent in the dye-doped sample. The electric field dependence of photoresponse data in P3HT-SQ fits $S(V) \propto F^n$, with $n = 2.0$–2.5, and this is associated with the quasi-equilibrium of carrier transit time and dielectric relaxation time. In the deconvoluted spectra of the P3HT-SQ sample, three Gaussian functions can fit the photoresponse data with modified peak profiles, which is associated with the redistribution of trap energetics. This shows that the presence of a small percentage volume of dye molecules enhances the energetics and charge transport in semiconducting polymers.

ACKNOWLEDGMENT

S.M. acknowledges the Department of Science and Technology, Government of India, for the INSPIRE fellowship (IF180122) to pursue PhD program.

[1] D. Fichou, Structural order in conjugated oligothiophenes and its implications on opto-electronic devices, J. Mater. Chem. **10**, 571 (2000).

[2] A. C. Grimsdale, K. Leok Chan, R. E. Martin, P. G. Jokisz, and A. B. Holmes, Synthesis of light-emitting conjugated polymers for applications in electroluminescent devices, Chem. Rev. **109**, 897 (2009).

[3] F. Zhang, D. Wu, Y. Xu, and X. Feng, Thiophene-based conjugated oligomers for organic solar cells, J. Mater. Chem. **21**, 17590 (2011).

[4] M. Ramuz, L. Bürgi, C. Winnewisser, and P. Seitz, High sensitivity organic photodiodes with low dark currents and increased lifetimes, Org. Electron. **9**, 369 (2008).

[5] J. Choi, H. Song, N. Kim, and F. S. Kim, Development of n-type polymer semiconductors for organic field-effect transistors, Semicond. Sci. Technol. **30**, 064002 (2015).

[6] T.-H. Le, Y. Kim, and H. Yoon, Electrical and electrochemical properties of conducting polymers, Polymers **9**, 150 (2017).

[7] C. Sun, F. Pan, H. Bin, J. Zhang, L. Xue, B. Qiu, Z. Wei, Z.-G. Zhang, and Y. Li, A low cost and high performance polymer donor material for polymer solar cells, Nat. Commun. **9**, 743 (2018).

[8] U. Kalsoom, A. Peristyy, P. Nesterenko, and B. Paull, A 3D printable diamond polymer composite: A novel material for fabrication of low cost thermally conducting devices, RSC Adv. **6**, 38140 (2016).

[9] G. Yu, K. Pakbaz, and A. Heeger, Semiconducting polymer diodes: Large size, low cost photodetectors with excellent visible-ultraviolet sensitivity, Appl. Phys. Lett. **64**, 3422 (1994).

[10] C. H. Lee, G. Yu, and A. J. Heeger, Persistent photoconductivity in poly(*p*-phenylenevinylene): Spectral response and slow relaxation, Phys. Rev. B **47**, 15543 (1993).

[11] I. G. Scheblykin, A. Yartsev, T. Pullerits, V. Gulbinas, and V. Sundström, Excited state and charge photogeneration dynamics in conjugated polymers, J. Phys. Chem. B **111**, 6303 (2007).

[12] Y.-M. Li, Phototransport under the presence of a small steady-state photocarrier grating, Phys. Rev. B **42**, 9025 (1990).

[13] See Supplemental Material at http://link.aps.org/supplemental/10.1103/PhysRevMaterials.8.075602 for transmission spectra comparison; schematic of measurements and equivalent circuit; experimental set-up.

[14] J.-S. Huang, T. Goh, X. Li, M. Y. Sfeir, E. A. Bielinski, S. Tomasulo, M. L. Lee, N. Hazari, and A. D. Taylor, Polymer bulk heterojunction solar cells employing förster resonance energy transfer, Nat. Photon. **7**, 479 (2013).

[15] P. J. Brown, D. S. Thomas, A. Köhler, J. S. Wilson, J.-S. Kim, C. M. Ramsdale, H. Sirringhaus, and R. H. Friend, Effect of interchain interactions on the absorption and emission of poly (3-hexylthiophene), Phys. Rev. B **67**, 064203 (2003).

[16] A. Roy, S. Mandal, and R. Menon, Lampert triangle formation and relaxation behavior in doped poly (3, 4-ethylenedioxythiophene) devices, J. Appl. Phys. **129**, 195501 (2021).

[17] A. Karki, G.-J. A. Wetzelaer, G. N. M. Reddy, V. Nádaždy, M. Seifrid, F. Schauer, G. C. Bazan, B. F. Chmelka, P. W. Blom, and T.-Q. Nguyen, Unifying energetic disorder from charge transport and band bending in organic semiconductors, Adv. Funct. Mater. **29**, 1901109 (2019).

[18] H. T. Nicolai, M. Kuik, G. Wetzelaer, B. De Boer, C. Campbell, C. Risko, J. Brédas, and P. Blom, Unification of trap-limited electron transport in semiconducting polymers, Nat. Mater. **11**, 882 (2012).

[19] M. M. Mandoc, B. de Boer, G. Paasch, and P. W. M. Blom, Trap-limited electron transport in disordered semiconducting polymers, Phys. Rev. B **75**, 193202 (2007).

[20] H. T. Nicolai, M. M. Mandoc, and P. W. M. Blom, Electron traps in semiconducting polymers: Exponential versus Gaussian trap distribution, Phys. Rev. B **83**, 195204 (2011).

[21] M. Jaiswal and R. Menon, Polymer electronic materials: A review of charge transport, Polym. Int. **55**, 1371 (2006).